Apatite as a pathfinder to tin mineralisation: prospects and caveats

Martin F. Mangler[1,*], Nicholas J. Gardiner[1], Dominic Skeat[1], Nick M. W. Roberts[2], Simon Tapster[2]

[1]School of Earth & Environmental Sciences, University of St Andrews, St. Andrews KY16 9TS, UK

[2]Geochronology and Tracers Facility, British Geological Survey, Nottingham NG12 5GG, UK

*Corresponding author. Email: mfm26@st-andrews.ac.uk

Abstract

Granite-related mineral deposits are major primary sources of the critical metals tin (Sn) and lithium (Li). The utility of accessory minerals such as zircon and apatite as pathfinders to these ore deposits has been a subject of great interest in recent years, with a number of geochemical discriminants having been developed to distinguish barren from metal-fertile and mineralised intrusions. Here, we study the prospects of apatite as an indicator mineral for tin and lithium mineralisation using a compilation of published apatite trace element data as well as new data for the mineralised Cornubian batholith and barren Bhutanese leucogranites. Critical examination of common geochemical discriminants tracing magma fractionation and redox conditions (Mn, Eu/Eu*, La/Yb_N and Sr/Y) shows large and overlapping data scatter for barren and Sn-fertile intrusions. This calls into question the utility of these petrogenetic indicators to pinpoint tin metallogeny, and it suggests that extreme fractionation and reduced conditions in S-type granites are necessary but insufficient conditions for tin mineralisation. Instead, *prima facie* metal concentrations directly related to tin mineralisation (i.e., Sn and Li) are consistently elevated in apatite from fertile and mineralised intrusions, which implies a critical role for source enrichment in tin metallogeny. Based on our data compilation, Li and Sn concentrations in apatite are the most robust indicators for Sn (and Li) mineralisation, and we encourage the community to include Li and Sn in their analytical routines to test this hypothesis further.

Keywords: Tin mineralisation; apatite; trace elements; exploration

1. Introduction

Apatite ($Ca_5(PO_4)_3(OH,F,Cl)$) is a common accessory mineral in magmas across the compositional spectrum. Its stability is primarily controlled by P concentrations in the magma, and it often appears early in the crystallisation sequence of granites (Hoskin et al., 2000; Piccoli and Candela, 2002; Broska et al., 2004; Macdonald et al., 2013; Miles et al., 2013; Zhang et al., 2021). Apatite can accommodate a range of key minor and trace elements such as REE, Sr, U, Pb, and Th (Belousova et

al., 2002; Mao et al., 2016); in particular, high apatite-melt partition coefficients for REE, Sr, and Y ($D_{ap/melt}$ ~3-10; Prowatke and Klemme, 2006) mean that apatite exerts significant control on the trace element budget of a magma during differentiation. Conversely, its wide stability field and compositional range make apatite a potentially powerful proxy through which to study evolving magma conditions and dynamics (Sha and Chappell, 1999; Miles et al., 2013; 2014; Stock et al. 2018; Li et al. 2021; Lormand et al., 2024; Xu et al. 2024). Moreover, apatite trace element compositions have been used to discriminate between different rock types, such as lherzolites, carbonatites, mafic rocks, granitoids, granite pegmatites, and iron oxides (Belousova et al., 2002), as well as S-type and I-type granites (Sha and Chappell, 1999), highlighting the utility of apatite in provenance studies.

Apatite is also a common accessory mineral in granite-hosted mineral deposits, and hence Belousova et al. (2002) highlighted the potential use of apatite as a resistate indicator mineral (RIM) in exploration for critical metals thanks to its widespread occurrence, wide stability field, relative resistance to weathering and surface processes, and ability to incorporate commodity elements such as Ni, Cu, Zn, and As. Since then, discriminant analysis of apatite has been used to distinguish magmatic-hydrothermal mineral deposits from unmineralised rocks (Mao et al., 2016) using a combination of Mg, V, Mn, Sr, Y, REE, Pb, Th, and U concentrations in apatite. The same authors also put forward characteristic apatite compositions for different mineralisation styles, including alkalic porphyry Cu-Au deposits, porphyry Cu ± Mo ± Au deposits, and Kiruna-type iron oxide apatite deposits (Mao et al., 2016). Similarly, Ding et al. (2015) distinguished between Cu-Pb-Zn porphyries and W-Sn-bearing granites by tracing the geochemical signatures of their respective magmatic sources (i.e., I-type vs S-type granites) in apatite.

Due to efforts to develop new metallogenic models for 'lithophile' granite-related magmatic-hydrothermal deposits, which host Sn, Li and other critical metals such as W and Ta, there has been growing interest in the use of accessory minerals as fertility indicators, which can be used to discriminate barren from metal-fertile deposits, and ultimately be used as pathfinders. Hence, a

small number of studies have recently examined the utility of apatite to explore for Sn mineralisation (Azadbakht et al., 2018; Guo et al., 2022; Li et al., 2022). These studies analysed trace elements in magmatic apatite from granitoids associated with Sn-mineralisation and concluded that Mn, Sr, Li, Sn, LREE/HREE and Eu/Eu* can be used to discriminate between Sn-fertile and barren magmas. However, these studies focused on specific case studies, and to date, no global compilation of trace element characteristics of apatite associated with Sn deposits has been produced.

Here, we compile published trace element data for apatite from barren and Sn-fertile igneous rocks, and we complement this with new apatite trace element data from Sn-mineralised units in the Cornubian batholith (SW England), as well as for barren 'Himalayan'-style leucogranites from Bhutan. We use the compilation to assess the fidelity of previously suggested trace element signatures in apatite to distinguish barren from Sn-fertile rocks, and we identify the geochemical discriminants which most robustly point towards tin mineralisation.

2. Geochemical discriminants in apatite

Geochemical discriminants developed for apatite are empirical in nature and aim to assess magmatic source, degree of fractionation, and oxidation state, since these petrogenetic constraints are considered to control the potential for granite-hosted mineralisation (Blevin and Chappell, 1992; Blevin et al., 1996; Černý et al., 2005, Gardiner et al., 2017). In particular, tin mineralisation is typically associated with highly fractionated, reduced granites derived from melting of crustal sediments (S-type; Taylor, 1979; Lehmann, 1982; Taylor and Wall, 1992; Romer & Kroner, 2016; Lehmann, 2021). Hence, the geochemical tracers proposed as pathfinders to tin mineralisation are those that pinpoint such high degrees of fractionation and low oxygen fugacity:

(1) **Sr** and **Y** in apatite are often used in combination to trace the degree of melt fractionation: Whilst Sr generally decreases during melt evolution due to plagioclase fractionation, Y is progressively enriched in the melt (Belousova et al., 2002). These trends in melt composition are thought to be reflected in apatite compositions. However, high melt (and hence apatite) Sr/Y

ratios may also reflect a high Sr/Y parental magma source, melting of a garnet-bearing source, or amphibole-dominated fractional crystallisation (Moyen, 2009; Nathwani et al., 2020).

(2) **La/Yb** and **other** ratios reflecting the slope of REE patterns also trace the degree of magma fractionation: whilst apatite generally show negative REE slopes, LREE/HREE ratios decrease by about two orders of magnitude during fractionation from primitive to highly evolved compositions; in pegmatites, REE slopes tend to be positive (i.e., LREE/HREE <1; Belousova et al., 2002). A primary reason for the LREE depletion is crystallisation of monazite or allanite, which preferentially incorporate LREE (Tepper and Kuehner, 1999; Miles et al., 2014; Li et al., 2022) thereby passively enriching HREE despite their slightly lower ap-melt partition coefficients (Prowatke and Klemme, 2006). Similar to all fractionation proxies, individual apatite La/Yb ratios therefore depend on the crystallising assemblage and its relative timing within the crystallisation sequence.

(3) **Eu anomalies (Eu/Eu*, where Eu* = $(Sm_N \cdot Gd_N)^{1/2}$)** are ubiquitously used proxies for magma fractionation in apatite (Belousova et al., 2002; Jia et al., 2020; Nathwani et al., 2020): negative Eu anomalies will increase during melt evolution due to plagioclase fractionation, which controls Eu/Eu* in apatite. As a result, the most evolved rocks are characterised by apatite with extreme Eu/Eu* <0.1 (Belousova et al., 2002). However, Miles et al. (2014) point out that Eu^{3+} is more compatible in apatite than Eu^{2+} (Prowatke and Klemme, 2006), and hence negative Eu anomalies could also reflect reducing magma conditions in addition to plagioclase fractionation. Unlike in zircon (Gardiner et al., 2017), Ce anomalies are rare in apatite (Belousova et al., 2002; Miles et al., 2014).

(4) **Mn** is **another** element that may reflect both fractionation and redox conditions: Manganese concentrations generally increase in the melt during fractionation, and increasing Mn concentrations in apatite are therefore often interpreted to reflect melt evolution (similar to Y); **Fe** displays analogous trends. However, Belousova et al. (2002) pointed out that Mn is also redox sensitive and that apatite in reduced magmas contains higher Mn concentrations due to the

increased availability of the more compatible Mn^{2+}. Based on this effect, Miles et al. (2014) suggested Mn in apatite as a redox proxy in silicic melts.

The utility of the above discriminants relies on the implicit assumption that extreme fractionation of S-type granites is sufficient to concentrate Sn enough to form mineralised deposits (Lehmann, 2021). However, as outlined above, a key commonality of such petrogenetic discriminants is that they are sensitive to several magmatic process and variables, and hence their petrogenetic significance is often ambiguous. Other discriminants target volatile compositions (i.e., **F** and **Cl** concentrations in apatite), but most studies find overlapping data and generally extreme enrichment in F and depletion in Cl (Ding et al., 2015; Mao et al. 2016; Azadbakht et al., 2018; Guo et al., 2022; Li et al. 2022). Halogen concentrations will therefore not be further considered in this study.

Less commonly, concentrations of the commodity metals themselves – e.g., **Sn** and **Li** concentrations – are reported for apatite. Recent studies indicate that apatite in igneous rocks associated with Sn mineralisation displays elevated Sn and Li concentrations (Azadbakht et al., 2018; Li et al., 2020; Guo et al., 2022), though to date there is not enough data to substantiate this finding. To this end, we analysed an additional 74 apatite crystals from barren and Sn-fertile rocks (n = 410 analyses), with particular focus on Sn and Li concentrations.

3. Materials and Methods

We compiled a dataset of published and new apatite trace element data obtained using laser ablation inductively coupled plasma mass spectrometry (LA-ICP-MS), with particular focus on Sn and Li concentrations in apatite. We categorised the apatite data into (i) *barren*: magmatic apatite from Sn-infertile intrusions); (ii) *Sn-fertile*: magmatic apatite from unmineralised regions of intrusions associated with tin mineralisation. These apatite crystals typically show no evidence for hydrothermal alteration; (iii) *Sn-mineralised:* apatite from altered, cassiterite-bearing regions of intrusions (including pegmatites, aplites and greisens). These apatite crystals have typically been affected by variable degrees of hydrothermal alteration.

In total, the dataset includes 343 datapoints for barren, 188 datapoints for Sn-fertile, and 136 datapoints for Sn-mineralised apatite. In addition, we compiled published apatite trace element data from Cu-fertile intrusions for reference (n = 460). The compiled data (Supplementary Material 1) was screened for outliers using a 3SD criterion, and results below detection limit are considered a zero result.

3.1 Published data

We compiled apatite trace element data from four studies (Azadbakht et al., 2018; Guo et al., 2022; Li et al., 2022; Ge et al., 2022). Apatite in the selected studies is described as magmatic in all cases, and they are either from barren or Sn-fertile intrusions. The literature compilation includes 109 apatite datapoints from Sn-fertile intrusions (three biotite granites from the Geiju Sn polymetallic district, China, Li et al., 2022; two biotite granites from the Dachang Sn polymetallic district, China, Guo et al., 2022; three biotite granites and one syenogranite from Acadia, Canada, Azadbakht et al., 2018) and 148 apatite datapoints from barren intrusions (one gabbro, one monzonite, and three biotite granites from the Dachang Sn polymetallic district, China, Guo et al., 2024; one gabbro-diorite from the Zhuxiling tungsten deposit, China, Ge et al., 2024; and three biotite granites from Acadia, Canada, Azadbakht et al., 2018). For comparison, we also compiled published data from magmatic apatite associated with Cu mineralisation (n = 460; Yang et al., 2018; Nathwani et al., 2020; Pan et al., 2020, 2021; Parra-Avila et al., 2022).

3.2 Additional samples

To ensure the representativeness of our global study on apatite as pathfinders to tin mineralisation, we performed additional analyses of apatite crystals from the fertile and mineralised portions of the Cornubian batholith as well as from three barren leucogranites from Bhutan (Supplementary Material 2). The Cornubian batholith samples include two Sn-fertile granites: a biotite granite (CW 02; n = 38) from the G3 series (Simons et al., 2016), and a G5 topaz granite (Tregonning granite; CW TREG; n = 41). In addition, apatite from an Sn-mineralised greisen deposit of the G2 muscovite series

(Cligga Head; CW 012; *n* = 100), and from an Sn-mineralised aplite from the G5 topaz series (Meldon aplite; CW MELAP; *n* = 36) were analysed. The barren Bhutanese leucogranites (n = 195) are ~15 Ma S-type granites related to melting of pelitic protoliths during the Himalayan orogeny (Hopkinson et al., 2017), and exhibited visible selvages of metapelitic material in the field.

3.3 Analytical methods

Apatite crystals for new analyses were separated from sieved whole rock samples (<250 µm fractions) via heavy liquid and magnetic separation before being mounted in epoxy resin. The mounts were imaged and analysed using a Jeol JXA-iSP100 electron microprobe and Jeol JSM-IT200 SEM at the University of St Andrews, UK, to aid targeting suitable crystals. Laser ablation ICP-MS analyses were conducted at the British Geological Survey Keyworth, UK using an ESL 193nm ImageGeo excimer laser ablation system connected to a Nu instruments Attom single-collector sector-field ICP-MS. Spot analyses were acquired using an ablation time of 12 s, a spot size of 30 µm, a repetition rate of 20 Hz, and a fluence of ~3 J/cm^2. Ablated material was carried by a 100% He gas composition in chamber before combining with a 50% argon mixture along the sample line. In apatite the following elements were measured: ^{7}Li, ^{27}Al, ^{29}Si ,^{31}P, ^{35}Cl , ^{44}Ca, ^{49}Ti, ^{63}Cu, ^{88}Sr, ^{89}Y, ^{98}Mo, ^{120}Sn, ^{139}La, ^{140}Ce, ^{141}Pr, ^{146}Nd, ^{149}Sm, ^{153}Eu, ^{157}Gd, ^{163}Dy, ^{166}Er, ^{172}Yb, ^{175}Lu, ^{177}Hf, ^{181}Ta, ^{186}W, ^{206}Pb, ^{232}Th, ^{238}U. Data reduction was performed in Iolite 3 (Paton et al., 2011) using the Trace Elements Data Reduction Scheme. Internal standardisation used an assumed stochiometric Ca concentration of 40.04 %, and NIST610 (Jochum et al., 2005) was used as the primary reference material. Data quality was monitored using reference materials Madagascar apatite, McClure apatite, Tiago apatite and Durango apatite. Relative standard deviations are typically between 5% and 20% for elements with concentrations ≥1ppm, and detection limits range between 5 ppb to 2 ppm (Supplementary Material 2). Full analytical details and data tables are provided in Supplementary Material 2.

4. Results

4.1 Trace elements in apatite: mean values

Mean trace elemental concentrations of apatite from Sn-fertile and Sn-mineralised rocks normalised to respective mean barren values are shown in Figure 1. Apatite in Sn-fertile rocks (Fig. 1a) show, on average, 3.3x lower Sr and 1.6x higher Y concentrations than apatite from barren intrusions, resulting in 18.6x lower Sr/Y values (mean Sr/Y = 0.04). Heavy REE are up to 3x higher in Sn-fertile apatite, whereas LREE concentrations are similar to barren values, resulting in 7.6x lower La/Yb_N values for Sn-fertile apatite (mean La/Yb_N = 2.5) compared to barren apatite (mean La/Yb_N = 18.9). In combination, these signatures appear to confirm a higher degree of fractionation for Sn-fertile intrusions. Slightly elevated Mn and Fe concentrations (enrichment factor of 1.6) as well as more pronounced negative Eu anomalies in apatite from Sn-fertile rocks (mean Eu/Eu* = 0.05) similarly point towards a higher extent of plagioclase fractionation than in barren intrusions (mean Eu/Eu* = 0.21). On the other hand, Li and Sn show the highest enrichment factors in apatite from Sn-fertile intrusions: on average, Li is 3.5x higher (mean Li = 21.1 ppm) and Sn is 16.8x higher (mean Sn = 9.6 ppm) than in apatite from barren rocks (mean Li = 6.1 ppm; mean Sn = 0.6 ppm). Mean Cu, Ga, As, Ba and W concentrations are enriched by a factor of 1.2 – 1.6 in apatite from Sn-fertile intrusions, and mean Pb, Th and U values are between 1.9 and 4.3x higher than in barren intrusions. No significant Ce anomaly is detected (Ce/Ce* = 1.08).

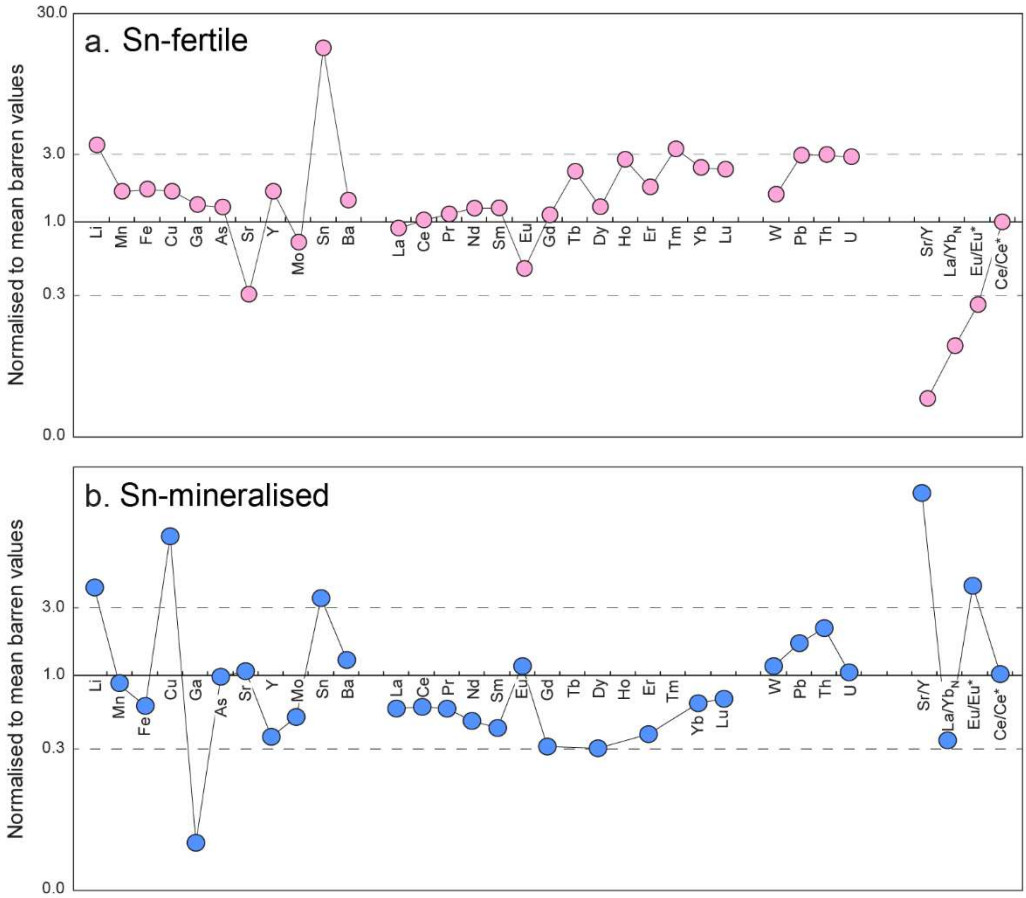

220

221 ***Fig.1****: Mean trace element concentrations in apatite from Sn-fertile and Sn-mineralised granitoids*
222 *relative to mean concentrations of apatite from barren rocks. Data compiled from Azadbakht et al.*
223 *(2018), Ge et al., (2022), Guo et al. (2024), Li et al. (2022), and this study. The most pronounced*
224 *differences between barren and Sn-fertile and -mineralised lithologies are found for Li, Sn, Eu/Eu*,*
225 *La/Yb_N, and Sr/Y.*

226 Apatite in Sn-mineralised rocks shows a general pattern of trace element depletion relative to mean
227 barren values (Fig. 1b). This observation is consistent with Bouzari et al. (2016) and Mao et al. (2016),
228 who found that apatite in hydrothermally altered rocks (i.e., hydrothermally altered magmatic
229 apatite or true hydrothermal apatite) has higher Ca concentrations and lower trace element
230 concentrations (REE, Y, Mn, Sr, Pb, Th, U) and suggested that this was due to trace element loss
231 during the hydrothermal stage. Our compilation supports their observation for REE, Y and Mn,
232 however mean Sr and U concentrations in apatite from Sn-mineralised rocks are indistinguishable

from barren ones, and Pb and Th concentrations are 1.7 and 1.4x higher, respectively (Fig. 1b). The rlative depletion of Y results in high Sr/Y ratios (mean Sr/Y = 14.5) compared to apatite from barren and Sn-fertile rocks. Overall REE slopes in apatite from Sn-mineralised intrusions are slightly steeper than in Sn-fertile rocks (mean La/Yb_N = 6.4), but La/Yb_N is 2.9x lower than in apatite from barren intrusions. Europium anomalies are weaker in apatite from Sn-mineralised rocks (Eu/Eu* = 0.88) than in apatite from barren and Sn-fertile intrusions, which may indicate oxidising conditions during mineralisation (e.g., Lehmann, 2021) or widespread feldspar dissolution. Consistent with Sn-fertile patterns, the most important enrichments in apatite from Sn-mineralised rocks are displayed for Li (4.1x enrichment), Sn (3.5x) and Cu (9.5x). Similar to the Sn-fertile samples, no significant Ce anomaly is observed (Ce/Ce* = 1.12).

4.2 Trace elements in apatite: data distributions

Mean concentrations can be misleading, particularly in case of skewed data distributions. Moreover, the utility of apatite as a pathfinder for tin mineralisation depends on data *ranges* (rather than means or medians) being distinguishable for different groups. In other words, a discriminant with distinct mean values but large scatter in each group is not a viable discrimination tool. For example, median Mn concentrations in apatite from barren, Sn-fertile, and Sn-mineralised rocks appear distinctive (Fig. 2a), but the data is heavily scattered for all three groups, producing widely overlapping concentration ranges. In fact, apatite from barren and Sn-fertile rocks shows almost identical upper and lower quartile ranges. As a result, if detrital apatite data were being examined with view to Sn mineralisation, Mn concentrations would not be a useful discriminant. Even apatite from Cu-fertile intrusions shows an overlapping range (yellow boxplot in Fig. 2a). A similar issue is present for La/Yb_N (Fig. 2b): while distinct mean and median values indicate that La/Yb_N in apatite is a useful tool to distinguish barren from Sn-fertile and -mineralised rocks, the range of data related to barren intrusions is large and substantially overlaps with Sn-fertile and -mineralised data, compromising its utility as a metallogenic discriminant. Better discrimination is achieved using Sr/Y (Sr shows similar results), where 75% of apatite from Sn-fertile intrusions have Sr/Y ≤0.029, while

83% of barren apatite have Sr/Y >0.029 (Fig. 2c; Supplementary Material 1). Tin-mineralised intrusions can also be distinguished from barren rocks using Sr/Y, as 75% of apatite in Sn-mineralised rocks have Sr/Y ≥0.13, whereas 75% of apatite in barren intrusions have Sr/Y ratios lower than that. Europium anomalies show a similar but less clear discrimination (Fig. 2d), with apatite from Sn-fertile rocks showing generally lower values (75% show Eu/Eu* ≤0.058) than those in barren rocks (68% show Eu/Eu* >0.058), and apatite from Sn-mineralised rocks showing generally higher values (75% show Eu/Eu* ≥0.18) than barren rocks (72% show Eu/Eu* <0.18).

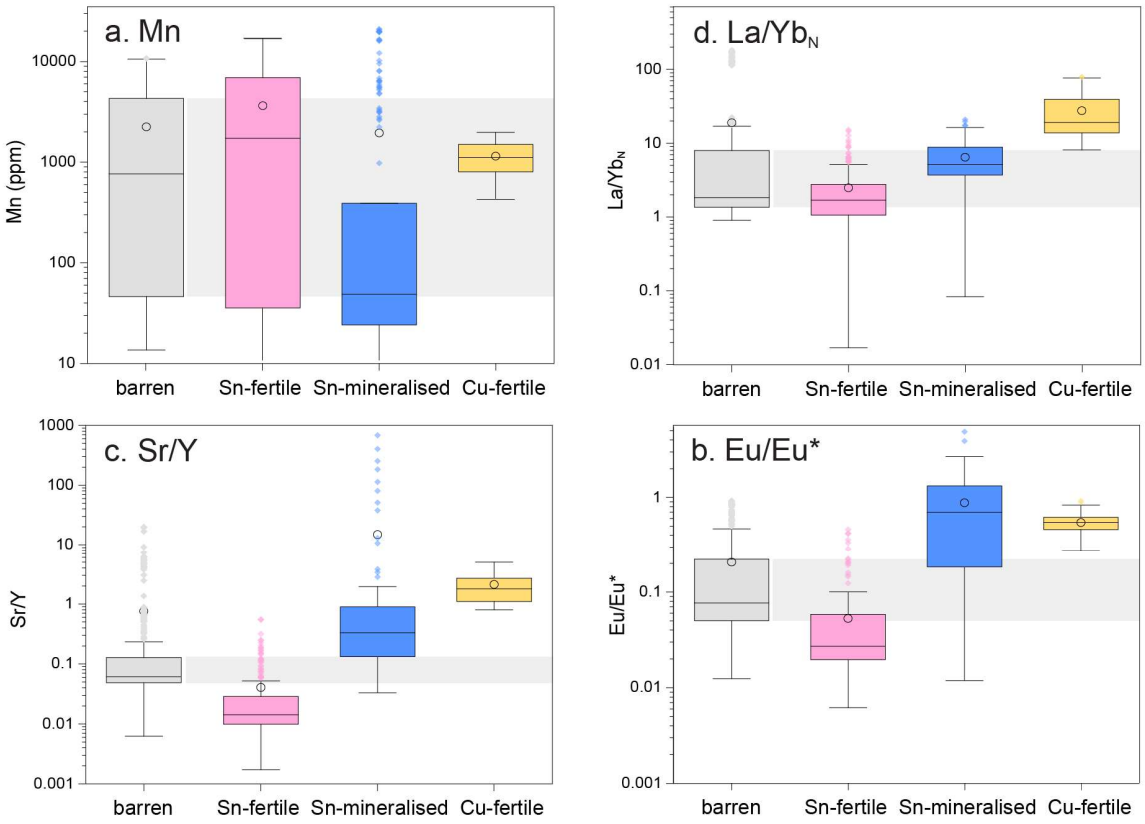

***Fig. 2**: Boxplots showing data distributions of four commonly used geochemical discriminants in apatite. Median (dashed lines) and mean (circles) values are distinct for apatite from barren, Sn-fertile and Sn-mineralised rocks, however their core (lower to upper quartile) ranges (boxes and grey areas) overlap significantly in many cases. This compromises the utility of Mn and La/Yb$_N$ to fingerprint tin mineralisation. Apatite from Cu-fertile intrusions generally exhibits distinct data ranges.*

This compilation shows that when entire data distributions are considered, established discriminants Mn and La/Yb_N in apatite are unreliable pathfinders for tin mineralisation. On the other hand, Sr/Y and Eu/Eu* signatures offer more robust discrimination, even though significant overlap remains at least in the case of Eu/Eu*. Finally, we note that Sr/Y and La/Yb_N can be used to identify magmatic apatite from Cu-fertile intrusions, as all three ratios are systematically higher than those of barren and Sn-fertile systems (Fig. 2).

In contrast to magma fractionation and redox proxies, metal concentrations in apatite directly related to tin mineralisation (Sn and Li) unambiguously distinguish between barren intrusions and those associated with tin mineralisation (Fig. 3). Specifically, Sn concentrations in apatite from Sn-fertile intrusions are consistently higher than those in barren rocks (Fig. 3a), with 75% of apatite from Sn-fertile intrusions showing Sn ≥1.3 ppm (maximum value: 59 ppm), whereas 97% of apatite from barren rocks show Sn <1.3 ppm (maximum value: 1.6 ppm). Apatite from Sn-mineralised rocks also display relatively elevated tin concentrations, with 75% showing Sn ≥0.8 ppm, which is higher than 80% of barren apatite.

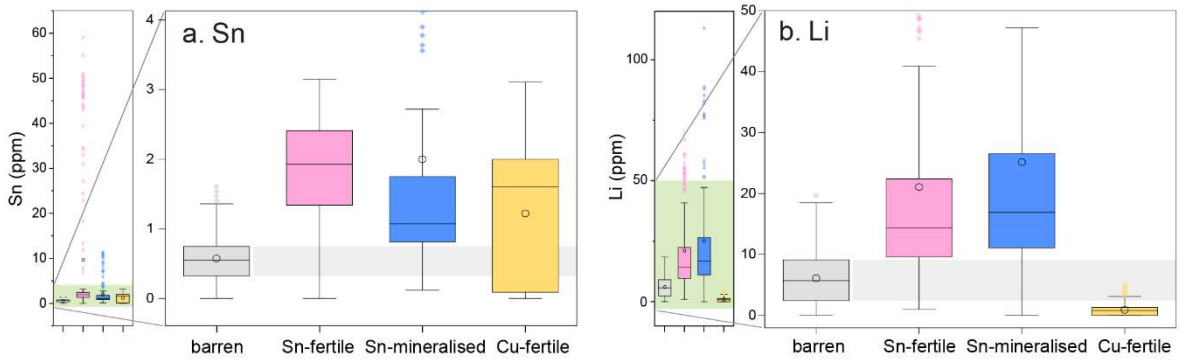

Fig. 3*: Boxplots showing data distributions of Sn and Li concentrations in apatite from barren, Sn-fertile, Sn-mineralised, and Cu-fertile rocks. The core ranges (lower to upper quartile = boxes and grey areas) of Sn and Li concentrations in apatite from barren intrusions are lower than those of Sn-fertile and Sn-mineralised apatite, facilitating robust discrimination between barren granitoids and those associated with tin deposits. Our data compilation further indicates that Li in apatite can also be used to identify Cu-fertile intrusions.*

Similarly, lithium shows distinctively high concentrations in both Sn-fertile and Sn-mineralised apatite (Fig. 3b): 75% of apatite from Sn-fertile and Sn-mineralised rocks show Li ≥9.7 ppm and Li ≥11 ppm, respectively, whereas 81% of apatite from barren intrusions have Li <9.7 ppm. Lithium and tin concentrations are therefore the most robust geochemical discriminants to fingerprint Sn mineralisation using both magmatic and hydrothermal (or hydrothermally altered) apatite. Based on our data compilation, Li in apatite can also be used to identify Cu-fertile intrusions (Fig. 3b).

5. Discussion

Our data compilation is consistent with our current understanding of tin metallogeny: the distinctly low Sr/Y and Eu/Eu* signatures of apatite from Sn-fertile intrusions confirm that Sn mineralisation requires a high degree of fractionation and reducing conditions. On the other hand, elevated Sr/Y and Eu/Eu* for apatite from Sn-mineralised rocks likely reflects removal of REE, Y and other incompatible elements under more oxidising conditions during hydrothermal alteration. However, beyond these first order trends, the data scatter for traditional geochemical discriminators is significant, and there remains significant overlap between barren and Sn-fertile and -mineralised rocks, in particular for Mn and La/Yb_N. Above all, this overlap between barren and Sn-fertile rocks speaks to the fact that extreme fractionation of reduced S-type granites (cf. Lehmann, 2021) is a *necessary* but, on its own, *insufficient* condition for tin mineralisation. Beyond this observation, which implies that source enrichment is a crucial factor controlling tin mineralisation (Romer & Kroner, 2015; 2016), the scatter in each group, as well as overlaps between barren and fertile groups may be due to a number of factors, which we discuss in the following section.

5.1 Petrogenetic and metallogenic ambiguity of apatite compositions

The wide ranges of Mn, Eu/Eu*, La/Yb_N and Sr/Y in apatite are not surprising given the multitude of source rocks, magmatic conditions and processes these geochemical proxies may represent. These include:

(1) *Source rocks and melt evolution histories are unique to each magmatic system.* Protoliths and melting conditions and degrees impart geochemical characteristics on a magma which may affect discriminants such as Sr/Y (Moyen, 2009; Roberts et al., 2024). Similarly, the geochemical evolution of a melt is controlled by its crystallisation sequence. Since apatite reflects evolving melt composition, trace element concentrations in apatite will vary depending on primary melt composition and crystallisation history (i.e., mineral phases which crystallise before or during apatite crystallisation). For example, the typical LREE depletion in apatite is controlled by crystallisation of monazite, allanite or titanite, which fractionate LREE (Tepper and Kuehner, 1999; Chu et al., 2009; Miles et al., 2013; Li et al., 2022). On the other hand, trends of decreasing Y and Yb concentrations in apatite of the Criffell granitic pluton in Scotland have been interpreted to represent zircon and earlier apatite crystallisation (Miles et al., 2013). Major mineral phases may also fractionate trace elements of interest, such as amphibole or biotite (Putzolu et al., 2024). Furthermore, apatite-melt partition coefficients can vary as a function of magmatic conditions; for example, Mn and Eu partition coefficients depend on redox conditions (e.g., Miles et al., 2014). Apatite trace element compositions therefore reflect igneous processes from source to final emplacement, and they will be different for each batch of magma.

(2) *Apatite crystals do not merely record the final stages of fractionation.* Apatite often appears early in the crystallisation sequence of silicic magmas, as evidenced by their common inclusion in rock-forming minerals (e.g., biotite, feldspar and zircon; Hoskin et al., 2000; Piccoli and Candela, 2002; Broska et al., 2004; Macdonald et al., 2013; Miles et al., 2013; Zhang et al., 2021; Li et al., 2022). Apatite may therefore record magma fractionation from early to late stage in any given rock sample, which will be reflected in its compositional range. This is useful to reconstruct magma petrogenesis but poses a problem from an exploration point of view: a rock from a Sn-fertile magma will likely contain apatite crystals which formed early (and long before mineralisation), and those crystals will therefore not reflect extreme fractionation; if such

apatite is then analysed as a detrital grain, it will not indicate tin mineralisation using petrogenetic discriminants such as Eu/Eu*, La/Yb_N or Sr/Y.

(3) *Diffusion and hydrothermal alteration may modify and obscure primary trace element concentrations.* Mineral-scale diffusion (>10 µm scale) in apatite at magmatic temperatures likely operates in timescales of days to decades for many elements (Ca, Pb, Sr, Mn, U, Li, F, Cl, OH; Cherniak, 2010). Diffusive re-equilibration of apatite with their host (melt or mineral) may therefore alter its trace element composition and obscure primary magmatic signatures. Similarly, fluid-moderated overprinting during and after the magmatic-hydrothermal transition may disturb or replace primary compositions. For example, Bouzari et al. (2016) found that hydrothermally altered apatite has higher Ca and lower trace element concentrations than apatite from unaltered rocks, which they attributed to trace element loss during alteration. If considered within its petrogenetic context, apatite can be an insightful tool to study these metasomatic processes (e.g., Harlov et al., 2015), but in an exploration context it adds an additional layer of complexity.

(4) *Apatite may host small inclusions of other minerals which may bias analyses*. For example, monazite and zircons inclusions are commonly observed in apatite (Tepper and Kuehner, 1999; Farley and Stockli, 2002). REE-rich minerals monazite and xenotime are often found as inclusions in hydrothermally altered apatite zones, where they likely formed in response to the metasomatic removal of REE from apatite (e.g., Harlov et al., 2005; 2011; Zirner et al., 2015). Larger inclusions may be avoided or detected in the ablation signal, but small, dispersed mineral or fluid inclusions may not be resolvable in the signal and bias the results.

In summary, common geochemical discriminants in apatite which empirically relate tin mineralisation to petrogenetic processes (e.g., fractionation and oxidation state) show large scatter because they record magmatic evolution over a temporal and spatial extent much beyond that of any mineralising process. Moreover, it indicates that barren and fertile granitoids undergo similar petrogenetic processes, which points towards source enrichment as a crucial pre-requisite for tin mineralisation.

5.2 Li and Sn as robust tracers of mineralisation

We argue that many common geochemical discriminants are petrogenetically ambiguous and often of limited use as robust discriminants for tin mineralisation. Instead, prima facie concentrations of Sn and Li in apatite offer a more satisfactory discrimination between barren granites and intrusions associated with Sn deposits (Figs. 3 & 4). This is a somewhat surprising result considering that apatite is not a primary host for either Li or Sn, which are more likely to be fractionated by micas (Ellis et al., 2022; Putzolu et al., 2024). Furthermore, Li is known to be a fast-diffusing element in most rock-forming minerals including apatite (Audétat et al., 2018, Li et al., 2020), which may obscure primary elemental signatures. This illustrates that Sn and Li are subject to the same processes that compromise the utility of common metallogenic indices, yet they retain distinctively elevated concentrations in apatite through differentiation.

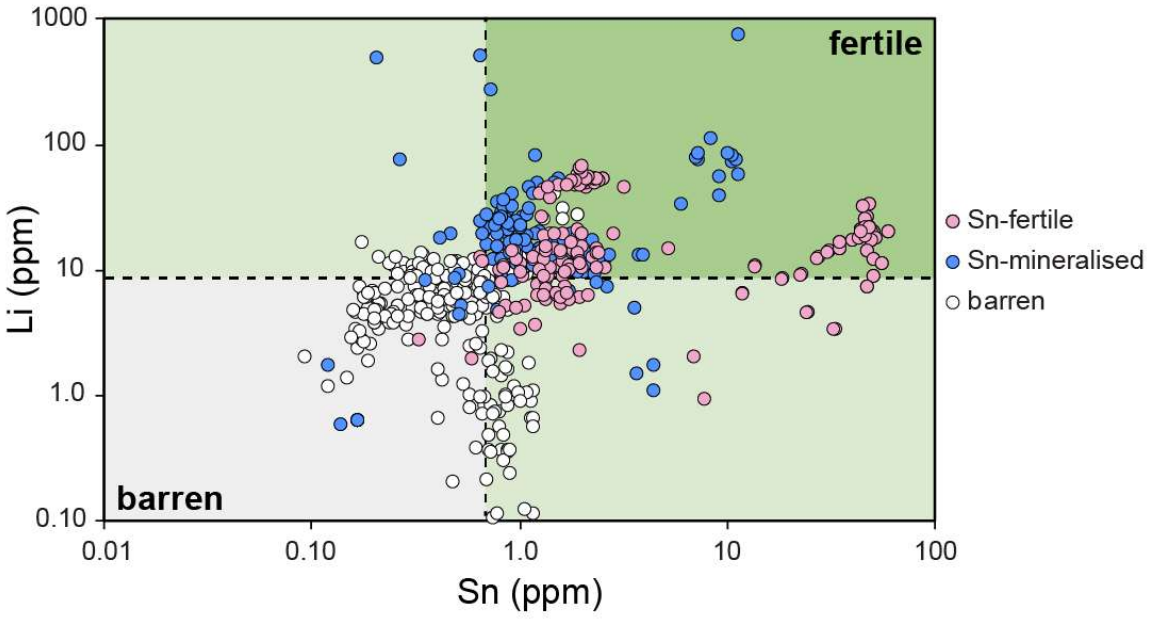

Fig. 4*: Lithium and tin concentrations in magmatic apatite from barren intrusions, Sn-fertile and Sn-mineralised intrusions. 75% of apatite from barren intrusions have Li ≤9.1 ppm and Sn ≤0.7 ppm, while >77% of apatite from Sn-fertile and -mineralised granitoids have Li >9.1 ppm, and >82% show Sn >0.7 ppm. This demonstrates the utility of Sn and Li concentration in apatite to fingerprint tin mineralisation.*

While we show that classical fractionation and oxidation indices fail to unambiguously point to Sn mineralisation, Li and Sn concentrations in apatite can "see through" complex petrogenetic and metallogenetic processes. This suggests that source enrichment and elevated primary Sn and Li concentrations are crucial aspects of tin mineralisation.

Our database shows that Sn and Li in apatite hold promise to be developed as robust discriminants for Sn mineralisation (Fig. 4). Specifically, apatite crystals with Li >9.1 ppm and Sn >0.7 ppm are highly likely to stem from a Sn-fertile or Sn-mineralised intrusion: 75% of apatite from barren granitoids fall below these thresholds, whereas 77% of apatite from Sn-fertile and 83% of apatite from Sn-mineralised rocks have higher Li concentrations, and 95% of apatite from Sn-fertile and 82% of apatite from Sn-mineralised rocks have higher Sn concentrations. For the new data presented in this study, mean analytical uncertainties are 22% (2SE) for Li and 13% for Sn (Supplementary Material 2); assuming more conservative uncertainties of 30% 2SE on analytical results dilutes the significance of the Li-Sn discriminant system. Despite this, based on our data compilation, we consider Li and Sn the most meaningful pathfinders to tin mineralisation using apatite.

6. Conclusions

Our apatite trace element data compilation reveals large variability of widely used geochemical fractionation and redox proxies for both barren, Sn-fertile and Sn-mineralised intrusions (Fig. 2), which leads to significant overlap between the groups. In part, this overlap implies that while extreme fractionation and reduced conditions in S-type granites are *necessary* conditions for tin mineralisation, they are, on their own, not *sufficient*. The much more distinctive character of Li and Sn concentrations in apatite (Figs. 3 & 4) indicates that source enrichment may be an additional precondition for tin mineralisation. These findings call into question the utility of petrogenetic indicators like Mn and La/Yb_N in tin exploration, at least for the case of apatite. Instead, our data suggests that Li and Sn in apatite are a more robust discriminant for Sn mineralisation. We therefore encourage the tin exploration community to exercise caution when using common petrogenetic

411 indicators (Mn, Eu/Eu*, La/Yb_N and Sr/Y), and we instead recommend including Sn and Li in their
412 apatite trace element analyses in order to optimise use of apatite as an indicator mineral for Sn
413 mineralisation.

414 Data Availability

415 All data underlying this study is available in the Supplementary Material.

416 Funding

417 MM and NJG thank the Leverhulme Trust for support (Research Project Grant RPG-2023-210).

418 References

419 Audétat, A., Zhang, L., & Ni, H. (2018). Copper and Li diffusion in plagioclase, pyroxenes, olivine and
420 apatite, and consequences for the composition of melt inclusions. Geochimica et Cosmochimica
421 Acta, 243, 99-115. https://doi.org/10.1016/j.gca.2018.09.016

422 Azadbakht, Z., Lentz, D. R., & McFarlane, C. R. (2018). Apatite chemical compositions from Acadian-
423 related granitoids of New Brunswick, Canada: implications for petrogenesis and
424 metallogenesis. Minerals, 8(12), 598. https://doi.org/10.3390/min8120598

425 Belousova, E. A., Griffin, W. L., O'Reilly, S. Y., & Fisher, N. I. (2002). Apatite as an indicator mineral for
426 mineral exploration: trace-element compositions and their relationship to host rock type. Journal of
427 Geochemical Exploration, 76(1), 45-69. https://doi.org/10.1016/S0375-6742(02)00204-2

428 Blevin, P. L., & Chappell, B. W. (1992). The role of magma sources, oxidation states and fractionation
429 in determining the granite metallogeny of eastern Australia. Earth and Environmental Science
430 Transactions of the Royal Society of Edinburgh, 83(1-2), 305-316.
431 https://doi.org/10.1017/S0263593300007987

Blevin, P. L., Chappell, B. W., & Allen, C. M. (1996). Intrusive metallogenic provinces in eastern Australia based on granite source and composition. Earth and Environmental Science Transactions of the Royal Society of Edinburgh, 87(1-2), 281-290. https://doi.org/10.1017/S0263593300006684

Bouzari, F., Hart, C. J., Bissig, T., & Barker, S. (2016). Hydrothermal alteration revealed by apatite luminescence and chemistry: A potential indicator mineral for exploring covered porphyry copper deposits. Economic Geology, 111(6), 1397-1410. https://doi.org/10.2113/econgeo.111.6.1397

Broska, I., Williams, C. T., Uher, P., Konečný, P., & Leichmann, J. (2004). The geochemistry of phosphorus in different granite suites of the Western Carpathians, Slovakia: the role of apatite and P-bearing feldspar. Chemical geology, 205(1-2), 1-15. https://doi.org/10.1016/j.chemgeo.2003.09.004

Černý, P., Blevin, P. L., Cuney, M. & London, D. Granite-related ore deposits. *Economic Geology 100th Anniversary Volume*, 337–370 (2005). https://doi.org/10.5382/AV100.12. https://doi.org/10.1017/S0263593300007987

Cherniak, D. J. (2010). Diffusion in accessory minerals: zircon, titanite, apatite, monazite and xenotime. Reviews in mineralogy and geochemistry, 72(1), 827-869. https://doi.org/10.2138/rmg.2010.72.18

Chu, M. F., Wang, K. L., Griffin, W. L., Chung, S. L., O'Reilly, S. Y., Pearson, N. J., & Iizuka, Y. (2009). Apatite composition: tracing petrogenetic processes in Transhimalayan granitoids. Journal of Petrology, 50(10), 1829-1855. https://doi.org/10.1093/petrology/egp054

Ding, T., Ma, D., Lu, J., & Zhang, R. (2015). Apatite in granitoids related to polymetallic mineral deposits in southeastern Hunan Province, Shi–Hang zone, China: Implications for petrogenesis and metallogenesis. Ore Geology Reviews, 69, 104-117. https://doi.org/10.1016/j.oregeorev.2015.02.004

Ellis, B. S., Neukampf, J., Bachmann, O., Harris, C., Forni, F., Magna, T., ... & Ulmer, P. (2022). Biotite as a recorder of an exsolved Li-rich volatile phase in upper-crustal silicic magma reservoirs. Geology, 50(4), 481-485. https://doi.org/10.1130/G49484.1

Farley, K. A., & Stockli, D. F. (2002). (U-Th)/He dating of phosphates: Apatite, monazite, and xenotime. Reviews in mineralogy and geochemistry, 48(1), 559-577. https://doi.org/10.2138/rmg.2002.48.15

Gardiner, N. J., Hawkesworth, C. J., Robb, L. J., Whitehouse, M. J., Roberts, N. M., Kirkland, C. L., & Evans, N. J. (2017). Contrasting granite metallogeny through the zircon record: A case study from Myanmar. Scientific reports, 7(1), 748. https://doi.org/10.1038/s41598-017-00832-2

Ge, L., Xie, Q., Yan, J., Huang, S., Yang, L., Li, Q., & Xie, J. (2024). Geochemistry of apatite from Zhuxiling tungsten deposit, eastern China: A record of magma evolution and tungsten enrichment. Solid Earth Sciences, 9(1), 100163. https://doi.org/10.1016/j.sesci.2024.01.001

Guo, J., Zhang, G., Xiang, L., Zhang, R., Zhang, L., & Sun, W. (2022). Combined mica and apatite chemical compositions to trace magmatic-hydrothermal evolution of fertile granites in the Dachang Sn-polymetallic district, South China. Ore Geology Reviews, 151, 105168. https://doi.org/10.1016/j.oregeorev.2022.105168

Harlov, D. E., Wirth, R., & Förster, H. J. (2005). An experimental study of dissolution–reprecipitation in fluorapatite: fluid infiltration and the formation of monazite. Contributions to Mineralogy and Petrology, 150, 268-286. https://doi.org/10.1007/s00410-005-0017-8

Harlov, D. E., Wirth, R., & Hetherington, C. J. (2011). Fluid-mediated partial alteration in monazite: the role of coupled dissolution–reprecipitation in element redistribution and mass transfer. Contributions to Mineralogy and Petrology, 162, 329-348. https://doi.org/10.1007/s00410-010-0599-7

Harlov, D. E. (2015). Apatite: A fingerprint for metasomatic processes. Elements, 11(3), 171-176. https://doi.org/10.2113/gselements.11.3.171

478 Hopkinson, T. N., Harris, N. B., Warren, C. J., Spencer, C. J., Roberts, N. M., Horstwood, M. S., &
479 Parrish, R. R. (2017). The identification and significance of pure sediment-derived granites. Earth and
480 Planetary Science Letters, 467, 57-63. https://doi.org/10.1016/j.epsl.2017.03.018

481 Hoskin, P. W., Kinny, P. D., Wyborn, D., & Chappell, B. W. (2000). Identifying accessory mineral
482 saturation during differentiation in granitoid magmas: an integrated approach. Journal of
483 Petrology, 41(9), 1365-1396. https://doi.org/10.1093/petrology/41.9.1365

484 Jia, F., Zhang, C., Liu, H., Meng, X., & Kong, Z. (2020). In situ major and trace element compositions of
485 apatite from the Yangla skarn Cu deposit, southwest China: Implications for petrogenesis and
486 mineralization. Ore Geology Reviews, 127, 103360. https://doi.org/10.1016/j.oregeorev.2020.103360

487 Jochum, K. P., Nohl, U., Herwig, K., Lammel, E., Stoll, B., & Hofmann, A. W. (2005). GeoReM: a new
488 geochemical database for reference materials and isotopic standards. Geostandards and
489 Geoanalytical Research, 29(3), 333-338. doi: 10.1111/j.1751-908X.2005.tb00904.x

490 Lehmann, B. (1982). Metallogeny of tin; magmatic differentiation versus geochemical
491 heritage. Economic Geology, 77(1), 50-59. https://doi.org/10.2113/gsecongeo.77.1.50

492 Lehmann, B. (2021). Formation of tin ore deposits: A reassessment. Lithos, 402, 105756.
493 https://doi.org/10.1016/j.lithos.2020.105756

494 Lormand, C., Humphreys, M. C., Colby, D. J., Coumans, J. P., Chelle-Michou, C., & Li, W. (2024).
495 Volatile budgets and evolution in porphyry-related magma systems, determined using
496 apatite. Lithos, 480, 107623. https://doi.org/10.1016/j.lithos.2024.107623

497 Li, W., Chakraborty, S., Nagashima, K., & Costa, F. (2020). Multicomponent diffusion of F, Cl and OH in
498 apatite with application to magma ascent rates. Earth and Planetary Science Letters, 550, 116545.
499 https://doi.org/10.1016/j.epsl.2020.116545

Li, W., Costa, F., & Nagashima, K. (2021). Apatite crystals reveal melt volatile budgets and magma storage depths at Merapi volcano, Indonesia. Journal of Petrology, 62(4), egaa100. https://doi.org/10.1093/petrology/egaa100

Li, J., Chen, S. Y., & Zhao, Y. H. (2022). Trace elements in apatite from Gejiu Sn polymetallic district: Implications for petrogenesis, metallogenesis and exploration. Ore Geology Reviews, 145, 104880. https://doi.org/10.1016/j.oregeorev.2022.104880

Macdonald, R., Bagiński, B., Dzierżanowski, P., & Jokubauskas, P. (2013). Apatite-supergroup minerals in UK Palaeogene granites: composition and relationship to host-rock composition. European Journal of Mineralogy, 25(3), 461-471. https://doi.org/10.1127/0935-1221/2013/0025-2291

Mao, M., Rukhlov, A. S., Rowins, S. M., Spence, J., & Coogan, L. A. (2016). Apatite trace element compositions: A robust new tool for mineral exploration. Economic Geology, 111(5), 1187-1222. https://doi.org/10.2113/econgeo.111.5.1187

Miles, A. J., Graham, C. M., Hawkesworth, C. J., Gillespie, M. R., Hinton, R. W., & Edinburgh Ion Microprobe Facility (EIMF) ionprobe@ ed. ac. uk. (2013). Evidence for distinct stages of magma history recorded by the compositions of accessory apatite and zircon. Contributions to Mineralogy and Petrology, 166, 1-19. https://doi.org/10.1007/s00410-013-0862-9

Miles, A. J., Graham, C. M., Hawkesworth, C. J., Gillespie, M. R., Hinton, R. W., & Bromiley, G. D. (2014). Apatite: A new redox proxy for silicic magmas?. Geochimica et Cosmochimica Acta, 132, 101-119. https://doi.org/10.1016/j.gca.2014.01.040

Moyen, J. F. (2009). High Sr/Y and La/Yb ratios: the meaning of the “adakitic signature”. Lithos, 112(3-4), 556-574. https://doi.org/10.1016/j.lithos.2009.04.001

Nathwani, C. L., Loader, M. A., Wilkinson, J. J., Buret, Y., Sievwright, R. H., & Hollings, P. (2020). Multi-stage arc magma evolution recorded by apatite in volcanic rocks. Geology, 48(4), 323-327. https://doi.org/10.1130/G46998.1

Pan, L. C., Hu, R. Z., Oyebamiji, A., Wu, H. Y., Li, J. W., & Li, J. X. (2021). Contrasting magma compositions between Cu and Au mineralized granodiorite intrusions in the Tongling ore district in South China using apatite chemical composition and Sr-Nd isotopes. American Mineralogist, 106(12), 1873-1889. https://doi.org/10.2138/am-2021-7497

Pan, L. C., Hu, R. Z., Bi, X. W., Wang, Y., & Yan, J. (2020). Evaluating magmatic fertility of Paleo-Tethyan granitoids in eastern Tibet using apatite chemical composition and Nd isotope. Ore Geology Reviews, 127, 103757. https://doi.org/10.1016/j.oregeorev.2020.103757

Parra-Avila, L. A., Hammerli, J., Kemp, A. I. S., Rohrlach, B., Loucks, R., Lu, Y., ... & Fiorentini, M. L. (2022). The long-lived fertility signature of Cu–Au porphyry systems: insights from apatite and zircon at Tampakan, Philippines. Contributions to Mineralogy and Petrology, 177(2), 18. https://doi.org/10.1007/s00410-021-01878-2

Paton, C., Hellstrom, J., Paul, B., Woodhead, J., & Hergt, J. (2011). Iolite: Freeware for the visualisation and processing of mass spectrometric data. Journal of Analytical Atomic Spectrometry, 26(12), 2508-2518. doi: 10.1039/C1JA10172B

Piccoli, P. M., & Candela, P. A. (2002). Apatite in igneous systems. Reviews in Mineralogy and Geochemistry, 48(1), 255-292. https://doi.org/10.2138/rmg.2002.48.6

Prowatke, S., & Klemme, S. (2006). Trace element partitioning between apatite and silicate melts. Geochimica et Cosmochimica Acta, 70(17), 4513-4527. https://doi.org/10.1016/j.gca.2006.06.162

Putzolu, F., Seltmann, R., Dolgopolova, A., Armstrong, R. N., Shail, R. K., Spratt, J., ... & Brownscombe, W. (2024). Influence of magmatic and magmatic-hydrothermal processes on the lithium endowment of micas in the Cornubian Batholith (SW England). Mineralium Deposita, 1-22. https://doi.org/10.1007/s00126-024-01248-5

547 Roberts, N. M., Hernández-Montenegro, J. D., & Palin, R. M. (2024). Garnet stability during crustal
548 melting: Implications for chemical mohometry and secular change in arc magmatism and continent
549 formation. Chemical Geology, 659, 122142. doi: 10.1016/j.chemgeo.2024.122142

550 Romer, R. L., & Kroner, U. (2015). Sediment and weathering control on the distribution of Paleozoic
551 magmatic tin–tungsten mineralization. Mineralium Deposita, 50, 327-338.
552 https://doi.org/10.1007/s00126-014-0540-5

553 Romer, R. L., & Kroner, U. (2016). Phanerozoic tin and tungsten mineralization—Tectonic controls on
554 the distribution of enriched protoliths and heat sources for crustal melting. Gondwana Research, 31,
555 60-95. https://doi.org/10.1016/j.gr.2015.11.002

556 Simons, B., Shail, R. K., & Andersen, J. C. (2016). The petrogenesis of the Early Permian Variscan
557 granites of the Cornubian Batholith: Lower plate post-collisional peraluminous magmatism in the
558 Rhenohercynian Zone of SW England. Lithos, 260, 76-94.
559 https://doi.org/10.1016/j.lithos.2016.05.010

560 Sha, L. K., & Chappell, B. W. (1999). Apatite chemical composition, determined by electron
561 microprobe and laser-ablation inductively coupled plasma mass spectrometry, as a probe into granite
562 petrogenesis. Geochimica et Cosmochimica Acta, 63(22), 3861-3881. https://doi.org/10.1016/S0016-
563 7037(99)00210-0

564 Stock, M. J., Humphreys, M. C., Smith, V. C., Isaia, R., Brooker, R. A., & Pyle, D. M. (2018). Tracking
565 volatile behaviour in sub-volcanic plumbing systems using apatite and glass: insights into pre-
566 eruptive processes at Campi Flegrei, Italy. Journal of Petrology, 59(12), 2463-2492.
567 https://doi.org/10.1093/petrology/egy020

568 Taylor, R.G., 1979. Geology of tin deposits, Developments in Economic Geology. Elsevier,
569 2032 Amsterdam.

570 Taylor, J. R., & Wall, V. J. (1992). The behavior of tin in granitoid magmas. Economic Geology, 87(2),
571 403-420. https://doi.org/10.2113/gsecongeo.87.2.403

572 Tepper, J. H., & Kuehner, S. M. (1999). Complex zoning in apatite from the Idaho batholith: A record
573 of magma mixing and intracrystalline trace element diffusion. American Mineralogist, 84(4), 581-595.
574 https://doi.org/10.2138/am-1999-0412

575 Xu, J., Xia, X. P., Wang, Q., Spencer, C. J., Zhang, L., & Zhu, X. (2024). Apatite textures, elemental and
576 isotopic compositions unmask the homogenizing process in silicic magma chambers. Geophysical
577 Research Letters, 51(2), e2023GL106646. https://doi.org/10.1029/2023GL106646

578 Yang, J. H., Kang, L. F., Peng, J. T., Zhong, H., Gao, J. F., & Liu, L. (2018). In-situ elemental and isotopic
579 compositions of apatite and zircon from the Shuikoushan and Xihuashan granitic plutons: Implication
580 for Jurassic granitoid-related Cu-Pb-Zn and W mineralization in the Nanling Range, South China. Ore
581 Geology Reviews, 93, 382-403. https://doi.org/10.1016/j.oregeorev.2017.12.023

582 Zhang, L., Chen, Z., Wang, F., & Zhou, T. (2021). Apatite geochemistry as an indicator of petrogenesis
583 and uranium fertility of granites: A case study from the Zhuguangshan batholith, South China. Ore
584 Geology Reviews, 128, 103886. https://doi.org/10.1016/j.oregeorev.2020.103886

585 Zirner, A. L., Marks, M. A., Wenzel, T., Jacob, D. E., & Markl, G. (2015). Rare earth elements in apatite
586 as a monitor of magmatic and metasomatic processes: The Ilímaussaq complex, South
587 Greenland. Lithos, 228, 12-22. https://doi.org/10.1016/j.lithos.2015.04.013